THE ACCELERATION OF CHARGED PARTICLES IN INTERPLANETARY SHOCK WAVES*

M. E. PESSES**

Goddard Space Flight Center/NASA, Greenbelt, Md., U.S.A.

R. B. DECKER

The Johns Hopkins University Applied Physics Laboratory, Laurel, Md., U.S.A.

and

T. P. ARMSTRONG

Dept. of Physics and Astronomy, University of Kansas, Lawrence, Md., U.S.A.

Abstract. The theory and observations of energetic ion acceleration in interplanetary shock waves is reviewed. The shock acceleration of the solar wind plasma and particle transport effects are discussed. Suggestions are offered for future research in shock acceleration physics.

1. Introduction

Spacecraft observations near 1 AU and in deep space show that the phenomenon of ion acceleration in interplanetary shock waves is a widespread and common occurrence in the heliosphere. *In situ* studies of interplanetary shock acceleration, besides contributing to our knowledge of the dynamic processes present in the solar wind, greatly facilitate our understanding of particle acceleration processes that occur in flare-produced shock waves, the terminal heliosphere shock and supernovae blast waves. Furthermore, the particle intensity enhancements produced by interplanetary shock acceleration are excellent diagnostic tools for studying charged particle propagation, since the characteristics of both the injected particles and the transport medium are directly observed.

The microphysics of the mechanisms capable of accelerating energetic charged particles to relativistic energies are now very well understood. However, how thermal particles are accelerated in shock waves, the particle transport physics during the acceleration process and the effects of nonplanar local and global shock geometries are not well understood.

Our purpose in this paper is twofold: (1) to review the microphysics of nonthermal particle acceleration in magnetostatic shock waves, and (2) to discuss recent work on some remaining unanswered questions of interplanetary shock acceleration.

2. Review of the Observations

The enhancements of energetic charged particle intensities produced by the interplanetary shock acceleration process are classified into three types.

* An invited paper presented at STIP Workshop on Shock Waves in the Solar Corona and Interplanetary Space, 15–19 June, 1980, Smolenice, Czechoslovakia.

** NAS/NRC Research Associate.

Space Science Reviews **32** (1982) 185–204. 0038–6308/82/0322–0185$03.00.

Those enhancements produced by shock waves generated by solar flares are called energetic storm particle (ESP) events. These events are observed only during the decay phase of solar flare ion events.

Enhancements produced by the shock waves that bound the solar wind stream-stream corotating interaction regions (Smith and Wolfe, 1977) are called corotating particle events (CPE). The CPE are usually observed at both the leading and trailing edges of the corotating interaction regions (CIR). The CPE can extend outward from the CIR for several AU, but are not observed inside the inner third of the interaction regions.

TABLE I

Average features of interplanetary Shock events

Features	ESP events	Corotating particle events	Shock spike events
Anisotropies at ~ 1 MeV/A: (A = number of nucleons)	Upstream: strong, anisotropic, field-aligned flow away from shock. Downstream: anisotropic flow away from shock, peaked $\sim \perp$ to field.	Same as ESP.	Same as ESP.
Particle intensity vs ψ_i:	Increases as ψ_i increases.	Same as ESP.	Same as ESP.
vs energy:	Lowest energies peak downstream, intermediate energies peak at shock, highest energies peak upstream.	Same as ESP.	Most peaks occur downstream, others occur at shock.
peak/background:	Decreases with increasing energy/A.	Same as ESP.	Same as ESP.
Energy spectra dJ/dE:	$v^n e^{-v/v_0}$ $(n = 0 \rightarrow 3)$ or $E^{-\gamma}$.	$v^2 e^{-v/v_0}$, $v_{0H} > v_{0He}$.	?
E_{max}:	~ 45 MeV/A. 1 case > 600 MeV/A. 1 case > 1 GeV/A.	~ 20 MeV/A.	~ 10 MeV/A.
E_{min}:	Solar wind energies.	< 30 keV/nucleus.	< 100 keV/A (probably much less).
Composition	H, He and heavy ions up to Fe present. Relative abundances unknown.	Similar to solar wind.	H, He, and CNO observed. Relative abundances unknown.
Electron events $E \gtrsim 40$ keV	2 reported in 18 years of observations.	1 reported in 7 years of observations.	0 reported in 15 years of observations.
Duration	~ 6–12 hr at 1 AU.	~ 12 hr–3 days outside 1 AU.	~ 30 min–3 hr at 1 AU.
Location	Observed 0.3–16 AU.	Observed 0.3–20 AU.	Observed 0.3–2 AU.

Those enhancements that are observed in the vicinity of 1 AU and that are: (a) associated with some type of interplanetary shock (either flare-produced or corotating); (b) not superposed upon and not produced by acceleration of a high-intensity background of solar flare particles (such as ESP events); and (c) characterized by relatively short-lived intensity spikes near the shock, are called shock spike events (SSE).

All the shock waves observed to be associated with ESP events, CPE or SSE are, to our knowledge, of the magnetosonic fast-mode variety.

A detailed review of interplanetary shock event observations is beyond the scope of this paper. It will suffice for our purposes to briefly list the average features of the observations. The average features of ESP events, CPE and SSE are summarized in Table I. This summary is based upon observations reported in Armstrong *et al.*, 1977; Ipavich *et al.*, 1979; Decker, 1981; Decker *et al.*, 1981; Pesses and Decker, 1982; Pesses *et al.*, 1982; and the many references from the above papers. In Table I, ψ_1 is the acute angle between the shock normal ($\hat{n}$) and the upstream magnetic field vector ($\mathbf{B}_1$).

Table I shows that ESP events and CPE share more common features than do SSE and either ESP events or CPE. There are four features common to all three shock enhancement types:

(1) the strongly anisotropic, field-aligned particle flow away from the shock in the upstream region, and the anisotropic, peaked nearly perpendicular to the field, flow of particles away from the shock in the downstream region;

(2) the positive correlation between the size of the particle intensity enhancements and the size of ψ_1;

(3) the extreme rarity of electron events at energies $\gtrsim 40$ keV; and

(4) the absence of particle enhancements associated with magnetostatic slowmode shock waves.

3. Review of Acceleration Microphysics for Energetic Particles

As seen by an observer moving with a magnetosonic fast-mode shock wave, the plasma enters (leaves) the shock front at a speed greater (less) than the local fast-mode magnetosonic wave speed, and the flow speed on either side of the shock exceeds the local Alfvén speed. As seen by an observer moving with a magnetosonic slow-mode shock wave, the plasma enters (leaves) the shock mode front at a speed greater (less) than the local magnetosonic slow-mode wave speed, and the flow speed on either side of the shock is less than the local Alfvén speed.

The incoming plasma is decelerated, compressed and heated in the shock front over a distance $\sim$ several thermal ion gyroradii. The very large gradients in $|\mathbf{B}|$ and the plasma bulk velocity that occur at the shock front combined with the induced electric field that exists in the shock rest frame are responsible for the acceleration of energetic (kinetic energy $\gg$ mean thermal energy) charged particles in shock waves

A. Shock Drift Mechanism

In the rest frame of nonparallel ($\psi_1 \neq 0°$) magnetostatic shock waves there exists a $\mathbf{V} \times \mathbf{B}$ electric field $\mathbf{E}_t$ due to the motion of the upstream and downstream magnetized plasma.

For the shock geometry in Figure 1(b), $\mathbf{E}_t = -\hat{y}|\mathbf{V}_{ss}|\,|\mathbf{B}_1|\sin\psi_1$, where $\mathbf{V}_{ss}$ is the shock velocity in the upstream plasma rest frame. As pointed out by Chen and Armstrong (1975), the $\nabla|\mathbf{B}|$ guiding center drift direction of ions (electrons) interacting with fast mode shock waves is parallel (antiparallel) to $\mathbf{E}_t$. Hence, the $\nabla|\mathbf{B}|$ at the shock front drives a current $\mathbf{J}$ and the particles comprising that current experience a $\mathbf{J}\cdot\mathbf{E}_t$ energy gain.

The magnitude of $\mathbf{B}$ downstream of slow-mode shock waves is smaller than the magnitude of $\mathbf{B}$ upstream, the reverse of the fast-mode shock case. Because of this difference, Pesses (1982) pointed out that the current driven by the $\nabla|\mathbf{B}|$ in slow-mode shock waves is antiparallel to $\mathbf{E}_t$. Hence in the rest frame of slow-mode shocks particles comprising the $\nabla|\mathbf{B}|$ current $\mathbf{J}$ experience a $\mathbf{J}\cdot\mathbf{E}_t$ energy loss.

The shock drift acceleration mechanism is not a Fermi process (Fermi, 1949). Fermi acceleration is due to the interaction of the particle's gyration velocity with the curl of $\mathbf{E}$ produced by a time-varying magnetic field (Northrop, 1963). As viewed from the shock frame, the shock drift acceleration results when the particle's cross-field drift velocity has a component parallel to the d.c. component of an electric field.

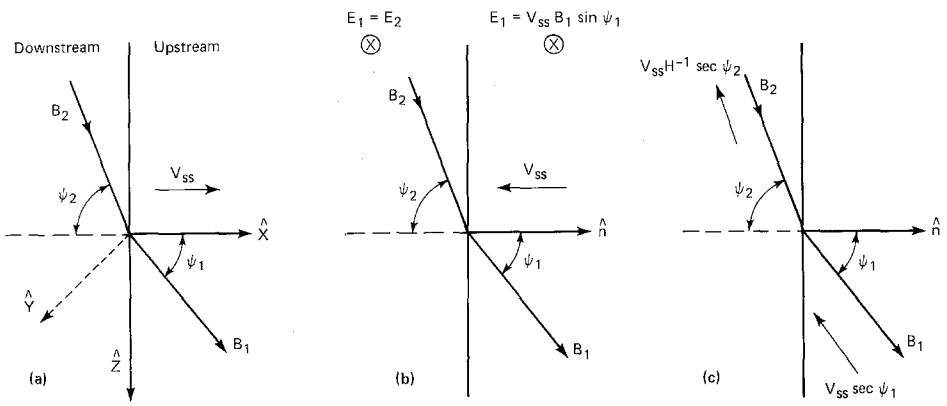

Fig. 1. (a) Upstream and downstream plasma rest frame, (b) Shock rest frame, (c) $\mathbf{E} = 0$ frame.

B. Compression Mechanism

The effect upon particle acceleration of the difference across the shock front in the plasma bulk flow velocity was pointed out independently by Axford *et al.* (1977) and Bell (1978). In the shock rest frame, particles that diffuse back and forth across the shock are accelerated by reflection off approaching upstream scattering centers and decelerated by reflection off receding downstream scattering centers. The scattering centers are convected by the bulk plasma motion, with the approaching scattering centers moving faster than the receding ones. Therefore, particles gain a net amount of energy by being effectively compressed between upstream and downstream scattering centers. This compression mechanism is a Fermi process and is physically distinct from the shock drift mechanism.

C. POST-SHOCK ENERGIES AND PITCH ANGLES

Given any planar magnetosonic shock wave that satisfies $|\mathbf{V}_{ss}| \sec \psi_1 <$ (the speed of light), there exists an inertial frame in which both the upstream and downstream $\partial \mathbf{B}/\partial t$ and $\mathbf{V} \times \mathbf{B}$ electric fields are simultaneously zero. In the $\mathbf{E} = 0$ (EEZ) frame shown in Figure 1(c), the plasma bulk velocity is along $\mathbf{B}$. Charged particles do not gain energy from the shock in the EEZ frame.

For fast and slow mode shock waves that are planar in the X-Z plane of Figure 1(a) and for which $\mathbf{V}_{ss}$, ψ_1 and ψ_2 (angle between $\hat{n}$ and downstream magnetic field $\mathbf{B}_2$) do not vary in space or time, the energy gains and pitch angle changes that result from both the shock drift and compression mechanisms can be calculated analytically provided that the post-shock pitch angle in the EEZ frame is known. The effects of the shock drift (compression) mechanism are calculated by transformations between the shock rest frame and the EEZ frame (the pre- and post-shock plasma rest frame of the particle). For calculations involving the effects of compression, it is assumed that the scattering centers are at rest in the plasma rest frame.

The scale length of the change in $|\mathbf{B}|$ in nonparallel magnetosonic shock fronts is much smaller than energetic particle gyroradii. Thus an extrapolation from the adiabatic theory of charged particle motion (Northrop, 1963) suggests that the adiabatic reflection law is not applicable to magnetosonic shock waves. However, numerical studies have shown that in the EEZ frame of oblique shocks (Pesses, 1982) and in the rest frame of perpendicular ($\psi_1 = 90°$) shocks (Parker, 1958, Pesses, 1981) the pre-shock and post-shock values of the particle's magnetic moment μ are equal for both transmitted and reflected particles when averaged over gyrophase for an initially gyrotropic distribution. The numerical studies also show that, as expected from the extrapolation of adiabatic theory, μ is not a constant of the motion during the shock interaction. For perpendicular shocks (Pesses, 1981) has shown that the equality between the pre- and post-shock values of μ for energetic particles is a result of the continuity of the angular momentum flux through the shock front. The same explanation is probably applicable in the case of oblique shock waves.

The expressions for the single shock encounter (one encounter involves many shock crossings) post-shock energies, pitch angles and pitch angle boundaries between reflected and transmitted nonrelativistic particles for magnetosonic fast-(slow) mode shock waves calculated under the assumptions discussed in the previous paragraph (i.e., particle reflection and transmission is adiabatic in the EEZ frame) are shown in the top (bottom) half of Table II. The expressions for fast-mode shock waves are from Pesses (1982), and the expressions for slow mode shock waves are presented here for the first time. The fractional energy change per nucleon for ions and per particle for electrons is given in Table II by $\Delta T/T_i = (T_{\text{final}} - T_{\text{initial}})/T_{\text{initial}}$, where the final and initial kinetic energies are evaluated in the plasma rest frame of the particle. The particle's final (initial) pitch angle is $\alpha_f(\alpha)$ and is evaluated in the plasma rest frame of the particle. Upstream of the shock $\alpha < (>) 90°$ if the particle is headed away from (towards) the shock. Downstream of the shock the reverse is true. Other quantities are defined as

TABLE II

Single encounter energy and pitch angle changes

	Reflected	Transmitted downstream	Transmitted upstream
Fast mode $\Delta T/T_i$:	$4R(R-\chi)$	$R\{R(J^2+1)-2\chi-2J[1+R(R-2\chi)-NS^2]^{1/2}\}$	$R\{R(J^2+1)-2J\chi+2[1+JR(JR-2\chi)-N^{-1}S^2]^{1/2}\}$
$\tan\alpha_f$:	$S(2R-\chi)^{-1}$	$N^{1/2}S\{JR-[1+R(R-2\chi)-NS^2]^{1/2}\}^{-1}$	$N^{-1/2}S\{R-[1+JR(JR-2\chi)-N^{-1}S^2]^{1/2}\}$
Pitch angle boundaries:	$R<1$: $RN^{-1}(1-A)<\chi<R$ $1\le R\le N^{1/2}$: $RN^{-1}(1-A)<\chi<RN^{-1}(1+A)$ $R\ge N^{1/2}$: no reflection $A\equiv[(N-1)(NR^{-2}-1)]^{1/2}$	$R<1$: $\chi<RN^{-1}(1-A)$ $1\le R\le N^{1/2}$: $\chi<\mathrm{RN}^{-1}(1-\mathrm{A})$ or $\chi>RN^{-1}(1+A)$ $R\ge N^{1/2}$: all transmitted For $\psi_1=90°$, $\Delta T/T_i=(N-1)S^2$, and $\tan\alpha_f=N^{1/2}S\chi^{-1}$ $J\equiv NH^{-1}$	$JR<1$: $\chi>JRN^{-1}\{1+[(N-1)(N(JR)^{-2}-1)]^{1/2}\}$ $JR\ge 1$: no transmission $R\equiv\lvert\mathbf{V}_{ss}\rvert\sec\psi_1\lvert\mathbf{V}\rvert^{-1}$ $M_A\equiv$ Alfvén Mach number $N^2=\cos^2\psi_1+\left(\frac{M_A^2-\cos^2\psi_1}{M_A^2-H\cos^2\psi_1}\right)^2H^2\sin^2\psi_1$ $H\equiv\rho_2/\rho_1$ $\chi\equiv\cos\alpha$, $S\equiv\sin\alpha$
Slow mode $\Delta T/T_i$:	$4JR(JR-\chi)$	$R\{R(J^2+1)-2\chi-2J[1+R(R-2\chi)-N^{-1}S^2]^{1/2}\}$	$R\{R(J^2+1)-2J\chi+2[1+JR(JR-2\chi)-NS^2]^{1/2}\}$
$\tan\alpha_f$:	$S(2JR-\chi)-1$	$N^{-1/2}S\{JR-[1+R(R-2\chi)-N^{-1}S^2]^{1/2}\}$	$N^{1/2}S\{R-[1+JR(JR-2\chi)-NS^2]^{1/2}\}^{-1}$
Pitch angle boundaries:	$JR<1$: $JR<\chi<JRN^{-1}(1+A)$ $JR\ge 1$: no reflection $A\equiv\{(N-1)[N(JR)^{-2}-1]\}^{-1/2}$	$R<1$: $\chi<R$ $R\ge 1$: *all transmitted* There are no slow mode shocks with $\psi_1=90°$ $J\cong NH^{-1}$	JR < 1: $\chi>\mathrm{JRN}^{-1}(1+\mathrm{A})$ $JR\ge 1$: no transmission $N\equiv\lvert\mathbf{B}_1\rvert\lvert\mathbf{B}_2\rvert^{-1}=N^{-1}_{\text{fast mode}}$

follows: R is the ratio of the projection of $\mathbf{V}_{ss}$ along $\mathbf{B}_1$ to the initial particle velocity $\mathbf{V}$, where $\mathbf{V}$ is evaluated in the plasma rest frame; J is the ratio of the downstream to upstream plasma bulk velocity in the EEZ frame; N is the magnetic shock strength (ratio of upstream to downstream magnetic field magnitude); and H is the hydrodynamic shock strength (ratio of downstream to upstream plasma number density). Note that the functional forms of R and H are the same for both fast- and slow-mode shocks, while those of J and N differ for the two modes. For fast-mode shocks only upstream particles are reflected; downstream particles are not. For slow-mode shocks the reverse is true. As an example in interpreting the information on pitch angle boundaries in Table II, particles are reflected from fast-mode shock waves when $R < 1$ if $RN^{-1}(1 - A) < \chi < R$, where $\chi = \cos\alpha$. All the expressions for $\Delta T/T_i$, and α_f and pitch angle boundaries are gyrophase averaged for a gyrotropic pre-shock distribution. The fast-mode equations in Table II are also discussed by Toptyghin (1980).

The agreement between the expressions given in Table II and calculations made by following exact particle trajectories numerically on a computer is excellent. Figure 2 compares analytical and numerical values of $\Delta T/T_i$ calculated for particles reflected and transmitted downstream by a fast mode shock wave, with $\psi_1 = 84°$, $|\mathbf{V}| = 20\,|\mathbf{B}_{ss}|$ and $N = 2$. The solid lines are analytical results and the circles are numerical calculations. For the numerical case, 25 particles equally spaced in gyrophase were used for each pitch angle. We note that in Figure 2 and Figure 2 only, the symbols R, T, and N denote reflected, transmitted downstream and noninteracting particles, respectively.

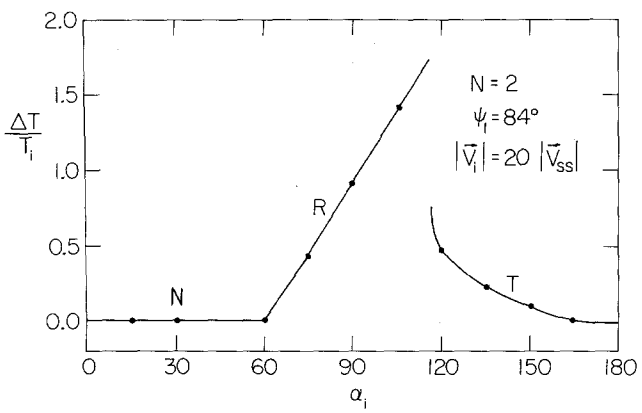

Fig. 2. Comparison between analytical predictions (solid lines) and numerical results (solid circles) for $\Delta T/T_i$ vs α.

The expressions in Table II are evaluated in a plasma rest frame. To transform these expressions to the spacecraft frame, one must perform the following transformations. For fast mode shock waves, $R \to R + (\mathbf{V}_{w1} \cdot \hat{n}) \cos\psi_1 |\mathbf{V}|^{-1}$ and $JR \to JR + (\mathbf{V}_{w2} \cdot \hat{n}) N^{-1} \cos\psi_1 |\mathbf{V}|^{-1}$. Here $\mathbf{V}_{w1}(\mathbf{V}_{w2})$ is the upstream (downstream) solar wind velocity in the spacecraft rest frame.

D. Comparison of Theory to Observation

The theory of energetic charged particle acceleration presented above can account for the four common features of shock events listed in Section 2.

(1) The transformations between the upstream (downstream) plasma rest frame and the EEZ frame is along $\mathbf{B}_1(\mathbf{B}_2)$ and does not affect the perpendicular velocity of the particle. Hence the pre- and post-shock values for the magnetic moment μ are also equal in the plasma rest frames. Particles reflected at fast-mode shocks therefore gain energy only in the parallel component. This accounts for the strongly anisotropic, field-aligned particle flow away from the shock in the upstream region. Particles transmitted at fast-mode shocks gain energy in the perpendicular component due to μ conservation and also gain energy in the parallel component due to the transformations out of the EEZ frame. This accounts for the anisotropic, peaked $\sim$ perpendicular to the field flow of particles away from the shock in the downstream region.

(2) Both the magnitude of $\mathbf{E}_t$ and the velocity of the $\nabla|\mathbf{B}|$ drift increase with increasing values of ψ_1. The drift time needed for reflected and transmitted particles to complete a single shock encounter also increases with increasing ψ_1. Thus, as the expressions in Table II show, $\Delta T/T_i$ increases as ψ_1 increases. The larger the energy gain per shock encounter, the larger the intensity enhancement observed by an integral detector. This accounts for the positive correlation between particle intensity enhancements and ψ_1. We note that $\Delta T/T_i$ does not become infinite as ψ_1 approaches 90° because for $R \geq N^{1/2}$ ($\geq J^{-1}$), there are no particles reflected (transmitted upstream) at fast-mode shocks. For similar reasons, $|\Delta T|$ is not smaller than T_i at slow-mode shocks.

(3) Because nonrelativistic particles interacting with magnetosonic shock waves pick up increments in velocity, the acceleration process scales as the particle velocity (energy per nucleon). A nonrelativistic electron with the same velocity as a proton has a kinetic energy 1836 times smaller. For instance, a 1 MeV proton and a 0.5 keV electron have nearly the same velocities. One reason why electron shock events are so rarely observed is because very few shocks are capable of accelerating ambient electrons above the $\sim$ 40 keV (corresponding to a velocity equal to that of a 90 MeV/nucleon ion) detector threshold. Another reason is that $\Delta T/T_i \propto |\mathbf{V}_{ss}|^2 |\mathbf{V}|^{-2}$. For a 1000 km s^{-1} flare shock in a 400 km s^{-1} solar wind, $|\mathbf{V}_{ss}| = 600$ km s^{-1}. Thus, for solar electrons with pre-shock energies $\sim 45-100$ keV, $|\mathbf{V}_{ss}|^2 |\mathbf{V}|^{-2} \sim 10^{-5}$, whereas for protons $\sim 0.5-1.0$ MeV, $|\mathbf{V}_{ss}|^2 |\mathbf{V}|^{-2} \sim 10^{-3}$.

(4) For slow-mode shocks the shock drift compression mechanism decelerates particles. Also the difference between the upstream and downstream plasma bulk velocities is several factors smaller than that for fast-mode shocks. This accounts for the absence of energetic particle enhancements associated with slow mode shocks.

4. Acceleration of Thermal Particles

Thermal ions pass through the shock too quickly to gain significant energy from the shock drift mechanism. Thermal electrons, because of their much larger gyrofrequency, can gain energy from this mechanism. However, Scott and Asses (1982) have shown that the

electrons that make up the shock front current sheet drift in the direction opposite to the direction of the electron $\nabla |\mathbf{B}|$ drift current. Only electrons with $\nabla |\mathbf{B}|$ drift velocities larger than the current sheet drift velocity gain energy from the shock drift mechanism. The lower energy threshold is the high velocity side of the electron thermal distribution. The compression mechanism may not be effective on thermal particles, since the magnetic field irregularities are convected by the thermal plasma.

Since neither the shock drift nor apparently the compression mechanisms are capable of effectively accelerating ions out of the solar wind, other mechanisms must be responsible for generating the superthermal ions observed downstream of ESP- and CPE-associated shock waves (Gosling *et al.*, 1980; Decker *et al.*, 1981).

The damping of plasma waves and turbulence in the post-shock flow (Gosling *et al.*, 1980) is a likely thermal shock-acceleration mechanism.

The ability of a fast-mode shock to accelerate thermal ions is believed to increase as ψ_1 decreases because the amplitude in downstream variations in **B** (and hence, in the energy available) for both interplanetary shock waves (Tsurutani, 1980) and the terrestrial bow shock (Greenstadt and Fredricks, 1979) increases as ψ_1 decreases. Another reason is that as ψ_1 decreases, the minimum velocity for downstream particles to overtake the shock also decreases.

5. Particle Transport

Pitch angle scattering of particles upstream and downstream of a shock results in particles undergoing spatial diffusion, convection and adiabatic deceleration. The energy spectra, intensity profiles and pitch angle distributions of the shock-produced energetic particle enhancements all depend upon the above transport processes.

A. Diffusion and Convection

The spatial diffusion coefficient D plays an important role in determining the number of times particles encounter the shock. When D is very large, particle guiding center motion dominates diffusion and convection, and in most cases the probability of a particle returning to the shock is very small. When D is very small convection dominates diffusion. *In the convective limit downstream particles cannot be scattered back to the shock, and the compression mechanism ceases to work in parallel shocks.* On the other hand, particles that are reflected upstream will not escape the shock, and are convected back to the shock. This is the situation in which the maximum number of shock encounters occurs for quasi-perpendicular shocks.

When the magnitude of D is such that diffusion is the dominant transport mechanism, the number of shock encounters depends upon the length of the shock front, the rate at which IMF lines are convected through the shock ($|\mathbf{V}_{ss}| \sin \psi_1$) and the mean free path parallel ($\lambda_\parallel$) and perpendicular ($\lambda_\perp$) to the mean interplanetary magnetic field (IMF) direction. For a particle to make multiple shock encounters, the IMF line along which the particle is diffusing must remain attached to the shock front. If $\lambda_\parallel$ is sufficiently large the connection to the shock could be broken by the time the particle is backscattered

towards the shock. This is more likely to happen to a downstream particle. Similarly, if $\lambda_\perp$ is large enough the particle can diffuse away from the field line connected to the shock.

For CIR shock waves, which extend from 1.5 AU to > 20 AU in the ecliptic and probably extend for several AU out of the ecliptic, the sizes of $\lambda_\parallel$, $\lambda_\perp$ and $|\mathbf{V}_{ss}| \sin \psi_1$ probably do not play important roles in determining the likelihood of multiple shock encounters. However, for shocks such as the earth's bow shock, the sizes of $\lambda_\parallel$, $\lambda_\perp$ and $|\mathbf{V}_{ss}| \sin \psi_1$ probably play essential roles in determining the number of shock encounters.

It is interesting to note that the spiral geometry and longevity ($\sim$ a few solar rotations) of CIR shocks allow for multiple shock encounters even in the limit of scatter-free ($\lambda_\parallel \to \infty$) particle motion along the mean spiral IMF. Particles reflected or transmitted upstream at the forward and reverse CIR shocks will mirror adiabatically in the inner solar system and return to the shock. For example, a 0.5 MeV proton that leaves a forward (reverse) shock at 4 AU with a pitch angle of 30° and heads toward the inner solar system in an upstream plasma having a speed of 400 km s^{-1} (650 km s^{-1}) will mirror and return to the shock in ~ 4 days (~ 3 days).

B. Adiabatic deceleration

The magnetic irregularities in the IMF that pitch angle scatter charged particles are convected by the solar wind's bulk motion and are receding from one another as the solar wind plasma expands outward from the Sun. Because of the relative recessional velocity of the irregularities, particles scattered by them undergo a net Fermi deceleration that is called adiabatic deceleration.

The adiabatic deceleration rate dT/dt is proportional to the divergence of the solar wind bulk velocity ($\mathbf{V}_{SW}$). For a spherically symmetric expansion, $dT/dt = -4 |\mathbf{V}_{SW}| T(3r)^{-1}$, where r is the heliocentric radial distance. For typical single encounter interaction times, $\sim$ 3–5 min for protons when $|\mathbf{B}| = 5\gamma$, the fractional change in kinetic energy due to adiabatic deceleration is only $\sim 10^{-3}$ (Pesses and Decker, 1982).

Plasma that enters the CIR through either the forward or reverse shocks is also compressed by the solar wind stream-stream interaction that produces the CIR (Smith and Wolfe, 1977, and references therein). The maximum solar wind density and pressure occurs in the middle of the CIR at the stream-stream interface (Smith and Wolfe, 1977). Thus the large, one to two orders of magnitude depressions in the energetic particle intensity observed in the middle of CIRs are not due to strong adiabatic cooling as Fisk and Lee (1980) have suggested.

C. Energy spectra

The energy spectra of shock-accelerated energetic particles can be calculated analytically if the energy gain per shock encounter averaged over incident pitch angle and the probability distribution function for the number of shock encounters are known.

Table II shows that the functional form of $\Delta T/T_i$ is different for reflected, transmitted upstream and transmitted downstream particles. Also, the range of pitch angles that are reflected or transmitted depends upon whether the particle is upstream or downstream and on the quantities R, N, and H. To account for these variations, the average energy gain per shock encounter $\langle \Delta T \rangle$ is defined as T_i multiplied by the weighted average of the three functional types of $\Delta T/T_i$, each of which have been averaged over the appropriate range of pitch angles. The weighting functions are the shock reflection, transmission downstream and transmission upstream coefficients. For the case in which $J \cong 1$ ($\psi_1 \gtrsim 70°$) and $R = |\mathbf{V}_{ss}|\,|\mathbf{V}_i|^{-1}$ *sec* $\psi_1 = V_T|\mathbf{V}_i|^{-1} \lesssim 1$ ($|\mathbf{V}_i|$ = initial particle speed), one finds (Pesses and Decker, 1982)

$$\frac{\langle \Delta T \rangle}{T_i} = c_1 R + c_2 R^2 + c_3 R^3 + 0[R^4] \tag{1}$$

where the constants c_1, c_2, and c_3 depend upon the magnetic field jump N and the pre-encounter pitch angle distribution. For pre-encounter particles that are initially upstream or downstream of the shock and distributed isotropically on a sphere in velocity space, $c_1 = 0.88$, $c_2 = 0.56$, and $c_3 = -0.04$ when $N = 2.0$.

As Equation (1) shows, energetic particles are most efficiently accelerated when $\psi_1 \sim 90°$ and the upstream and downstream IMF lines make small angles with the shock front. Conversely, as discussed in Section 4, thermal particles are apparently most efficiently accelerated to superthermal energies when $\psi_1 \lesssim 45°$ and the upstream and downstream IMF lines make large angles at the shock front. To accelerate thermal particles to high energies in fast-mode shocks it is apparently necessary for ψ_1 to oscillate between quasi-parallel and quasi-perpendicular configurations. If ψ_1 remains $\lesssim 45°$ for a prolonged period of time, particles cannot encounter the shock enough times to reach energetic levels because of the small values of $\langle \Delta T \rangle$. If ψ_1 remains $\sim 90°$ for a prolonged period of time, the superthermal particle source will eventually be exhausted.

An example of this ψ_1 variation is given in Figure 3, which shows high time resolution data for a reverse CIR shock observed at 2.1 AU from the Sun by the University of Iowa charged particle detectors and the Jet Propulsion Laboratory vector helium magnetometer on Pioneer 11. The upper panel gives one-minute averages of the IMF strength. The lower panel gives one-minute spin-averaged count rates of 0.6–3.4 MeV protons. The middle panel gives the absolute value of 90° minus ψ_1, the angle between the observed direction of the shock normal $\hat{n}$ and the reconstructed direction of the upstream IMF vector $\mathbf{B}_1$. $\mathbf{B}_1$ is reconstructed by using the shock jump conditions and assuming that the direction and magnitude of the field, $\hat{n}$ and the shock strength N do not vary with time or along the shock front.

The reconstructed value of ψ_1 fluctuates between $\lesssim 45°$ and $\sim 90°$. Spike-like structures in the counting rate coincide with the times when $\psi_1 \sim 90°$ ($|90° - \psi_1| \sim 0°$) as expected from the ψ_1 dependence on the shock acceleration process. For other CIR shock events observed by Pioneer 11, when $\psi_1 \sim 90°$ for prolonged periods downstream, only slight counting rate enhancements were observed, and not the spikelike enhance-

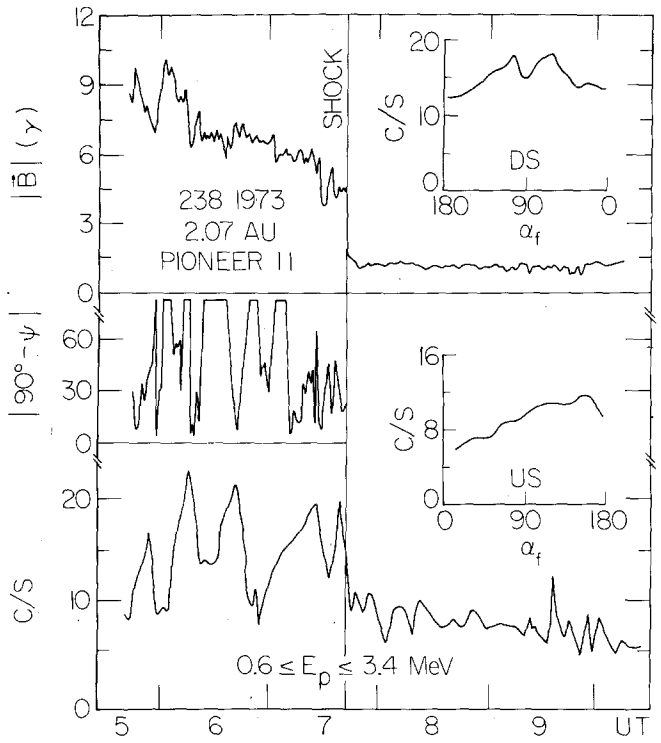

Fig. 3. One-minute averages of the IMF strength (top) and spin-averaged count rates of 0.6–3.4 MeV protons (bottom) observed at a reverse CIR shock event by Pioneer 11 at 2.07 AU. The middle panel gives the reconstructed absolute value of $90° - \psi_1$. The top (bottom) insert in the right-hand panel shows downstream (upstream) pitch angle distributions observed one hour preceding (following) the reverse shock passage.

ments seen when ψ_1 oscillates between $\lesssim 45°$ and $\sim 90°$ (Pesses *et al.*, 1982). This result is consistent with the expected ψ_1 dependence.

The boundaries between the regions where the IMF is nearly parallel to and nearly normal to the shock front can act as escape boundaries for particles diffusing inside the region where the field line is nearly parallel to the shock's surface (Pesses and Decker, 1982). The mean free path normal to the shock front is $\lambda_n = \lambda_\parallel \cos^2 \psi_i + \lambda_\perp \sin^2 \psi_i$, where the subscript $i = 1$ (2) if the particle is upstream (downstream) of the shock front. The 'ψ' boundary can act as an escape boundary because of the large change in λ_n that can occur there.

Particles diffusing inside an escape boundary have an exponential lifetime inside the bounded region (Parker, 1963). For an exponential lifetime the probability of a particle encountering the shock between n and $n + \mathrm{d}n$ times is (Pesses and Decker, 1982)

$$P(n)\,\mathrm{d}n = \langle n \rangle^{-1} \exp\left(-n \langle n \rangle^{-1}\right) \mathrm{d}n\,, \tag{2}$$

where $\langle n \rangle$ is the mean number of shock encounters. If $\lambda_\parallel \gg \lambda_\perp$ and $\lambda_\parallel$ is rigidity

independent, as several observational studies indicate (Zwickl and Webber, 1979), then $\langle n \rangle$ will not depend upon either the particle species or the initial particle energy in the region bounded by $\psi_1 \sim 90°$. If, however, $\lambda_\parallel$ is rigidity dependent, then $\langle n \rangle$ will depend on the particle species and the initial particle energy in the region bounded by $\psi_1 \sim 90°$.

The expression for the energy spectrum is found by combining (1) and (2) to give, to order $V^2 V_T^{-2}$ (V = particle speed),

$$J(T)\,\mathrm{d}T = KV^2 \exp(-VV_0^{-1})\,\mathrm{d}T, \tag{3}$$

where $J(T)\,\mathrm{d}T$ is the number of particles per unit time per unit area per unit solid angle with energy in the plasma rest frame between T and $T + \mathrm{d}T$, $V_T = |V_{ss}| \sec\psi_1$, $V_0 = 0.5c_1 \langle n \rangle V_T$, and K is a function of the pre-shock spectrum.

The e-folding velocity V_0 can depend upon particle species. Sarris and Van Allen (1974) pointed out that when ψ_1 varies with time the value of $\Delta T/T_i$ can depend upon the particle-shock interaction time. The value of ψ_1 usually remains $\sim 90°$ for only several minutes. Thus, particles with shock interaction times $\leq$ the time when $\psi_1 \sim 90°$ will be fully accelerated while the IMF is favorably oriented. Particles with longer acceleration times will also experience a period when the IMF is not favorably oriented, and will therefore gain less energy than the more quickly interacting particles. It can be shown from the dimensionless form of the Lorentz force equation that the particle-shock interaction time is proportional to the mass to charge ratio m/q. Therefore, if the time variations in ψ_1 are on the order of the proton acceleration time, which for reflecting particles is

$$\sim 8m(q|\mathbf{B}|)^{-1} N(N^2-1)^{-1} \sec\psi_1 \times \\ \times \{2\cos^{-1}[(\cos\alpha - R)(1 - 2R\cos\alpha + R^2)^{-1/2}] - \pi\},$$

then $\langle \Delta T \rangle$ will decrease as m/q increases. Hence V_0 for ${}_1H^{+1}$ will be larger than V_0 for ${}_4He^{+2}$, and V_0 for not fully stripped ions will be somewhere between that of ${}_1H^{+1}$ and ${}_4He^{+2}$.

Equation (3) can account for many of the CPE features. The CPE spectra observed by Gloeckler *et al.* (1979), Mewaldt (private communication, 1980), and McGuire *et al.* (1980) are of the form $\mathrm{d}J/\mathrm{d}T \propto V^2 \exp(-V/V^*)$, where V^* ranges from 2000 km s^{-1} to 6000 km s^{-1}, with a mean value of ~ 3000 km s^{-1}.

The observed average value of $|\mathbf{V}_{ss}|$ and N for CIR shocks are 150 km s^{-1} and 2.0, respectively (Smith and Wolfe, 1977). Using the mean values of $|\mathbf{V}_{ss}|$ and N, plus $\langle n \rangle$ = 5–7 and values of ψ_1 ranging from 81° to 87°, one reproduces the observed e-folding velocities.

Observations by McGuire *et al.* (1980) show that the e-folding velocity for ${}_1H^{+1}$ in CPE is significantly harder than that of ${}_4He^{+2}$. This is consistent with the m/q dependence of V_0 as discussed above.

Observations by Barnes and Simpson (1976) show that, on the average, the energy spectra (peak intensities) of the CPE associated with the reverse shocks at the trailing edges of CIRs are harder (larger) than the CPE associated with the forward shocks at

the leading edges of CIRs. The configuration of the IMF and the geometry of the CIR shocks are such that, on the average, ψ_1 for reverse shocks is expected to be larger than ψ_1 for forward shocks at equal heliocentric radial distances (Smith and Wolfe, 1977). No differences in $|V_{ss}|$ and N between forward and reverse shocks have been observed by Pioneers 10 and 11 (Pesses *et al.*, 1979). The above ψ_1 difference combined with the fact that $V_0 \propto \sec \psi_1$ can account for the CPE associated with reverse shocks being, on the average, harder than those associated with the forward shocks. Similarly, since $\langle \Delta T \rangle \propto \sec \psi_1$, particles interacting with reverse shocks will gain more energy per encounter than those interacting with forward shocks. This can account for the CPE associated with reverse shocks having, on the average, larger intensities than those associated with the forward shocks.

Observations at 1 AU of CPE associated with reverse CIR shocks show that the *e*-folding velocity increases with increasing time (Gloeckler *et al.*, 1979 and references therein). During a CPE at 1 AU the heliocentric radial distance r of the point on the CIR reverse shock to which an observer (located in the plasma upstream of the reverse shock) is magnetically connected increases with increasing time. Now the angle between the normal vector of an ideal corotating shock and the mean IMF spiral direction (ψ_1) increases with increasing r. This r dependence of ψ_1 combined with $V_0 \propto \sec \psi_1$ produces an *e*-folding velocity at 1 AU during a reverse shock CPE that increases with increasing time, as is observed.

Because ESP events occur during solar flare energetic particle events that provide a pre-existing superthermal and energetic particle population, the acceleration of solar wind thermal ions to superthermal energies is not required to eventually produce energetic ions by the ESP shock waves. Therefore, the efficient production of energetic particles does not require that ψ_1 oscillate between $\lesssim 45°$ and $\sim 90°$ as in the case of CPE and SSE. Hence, the energy spectra (e.g., Equation (3)) that result when such oscillations are necessary will not necessarily be observed in ESP events.

D. Intensity Profiles and Pitch Angle Distributions

The intensity enhancement profiles for seven consecutive low energy ion channels observed during an ESP event at ~ 1.65 AU by the Low Energy Charges Particle (LECP) experiment aboard Voyager 1 are shown in Figure 4. While the maximum intensity occurs near the shock for all energies, the relative abundance of particle enhancements upstream and downstream is strongly energy-dependent. At the lowest energies of 30–53 keV/ion, almost the entire enhancement is observed downstream of the shock. As the energy increases, the percentage of the particle enhancement that is upstream increases, with equal upstream and downstream fluxes occurring in the 139–220 keV/ion channel. Also note that the duration of the enhancement downstream decreases with increasing energy, while the duration upstream increases with increasing energy. Very similar energy-dependent intensity profiles are observed in ESP events at 1 AU and in CPE in deep space (Decker *et al.*, 1981, and references therein).

The upstream increase in event duration with increasing energy (i.e., the increase in the particle distribution scale lengths with increasing velocity) in Figure 4 is consistent

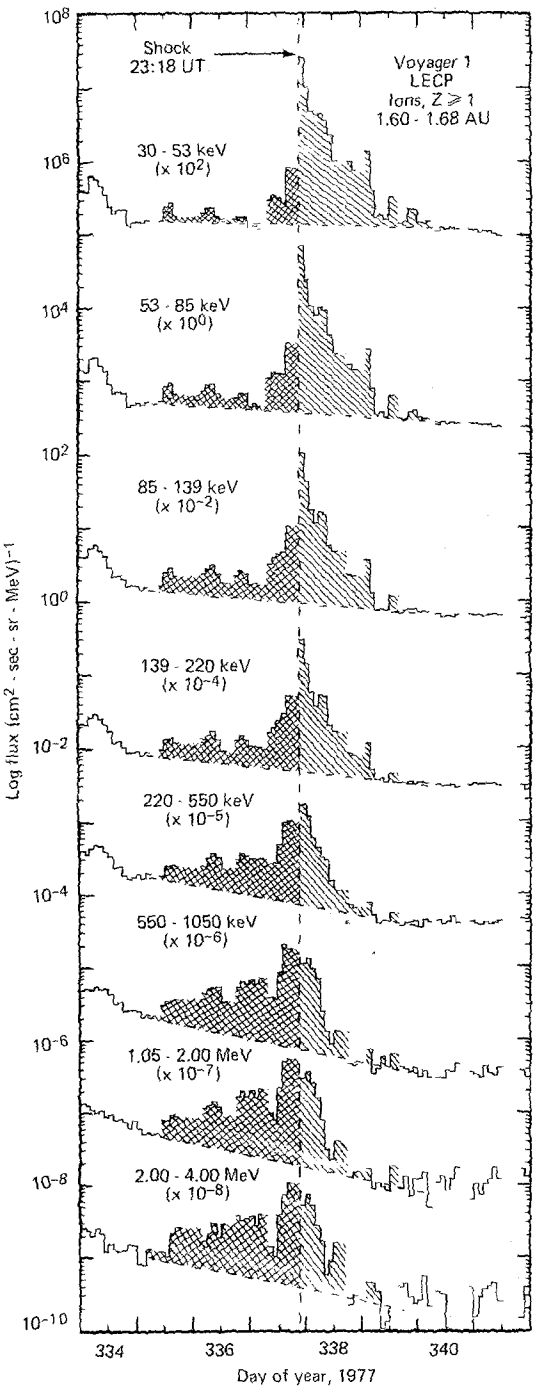

Fig. 4. Two-hour, scan-averaged fluxes from eight consecutive Voyager 1 Low Energy Charged Particle (LECP) experiment ion channels during the day of year 337, 1977 ESP event. The different shading in the upstream and downstream regions emphasizes the energy-dependence of the shock enhancement morphologies.

with multiple shock encounters and diffusive particle propagation, where $D \propto V^n$ and $n > 0$. However, the downstream decrease in event duration with increasing energy is inconsistent with a diffusively controlled intensity profile.

In some situations, a particle's acceleration at the shock combined with its scatter-free ($D = \infty$) adiabatic guiding center motion along a laminar spiral IMF can mock diffusive behavior in ESP events. Decker (1981) has studied the intensity enhancement profiles and pitch angle distributions produced by sun-centered spherical blast waves that propagate through an ambient energetic particle population. A computer simulation designed to trace particle orbits backwards in time from a specified observation point to the pre-shock-interaction point provides a full diagnosis as to which observed particles interacted with the shock, where the shock-particle interaction occurred and by how much each interacting particle's kinetic energy was increased. Particles are assumed to encounter the shock only once.

The simulation model correctly recovers the gross features of the intensity variations, flux anisotropies and energy spectra time evolutions of many observed ESP events. Representative simulation results predict shock-induced enhancements in low energy ($\lesssim 0.1$ to ~ 1.0 MeV) proton fluxes that are characterized by: (a) long, steady pre-shock or upstream rises to peaks before the shock arrival and abrupt declines following the shock passage; (b) peak enhancement amplitudes that increase for lower energy protons, stronger and faster shocks, softer ambient proton spectra, increased ψ_1 and increased radial distance from the Sun; (c) large, highly field-aligned pre-shock flux anisotropies directed away from the Sun along the IMF; (d) small post-shock flux anisotropies nearly perpendicular to the magnetic field and directed towards the Sun along the IMF; (e) steadily softening pre-shock energy spectra that are steepest at the peak flux enhancement and slightly softer than the ambient spectra after the shock passage.

For a spherical shock moving through a nominal spiral IMF, the value of ψ_1 at any point is the angle that the local IMF vector makes with the radial direction. For a 400 km s^{-1} solar wind, $\psi_1 \simeq 43°$ at 1 AU and increases towards the Sun. Such small ψ_1 values have been shown to produce relatively small peak enhancements (peak/background ~ 1.5) for $\lesssim 1$ MeV protons at 1 AU (Decker, 1979, 1981), as expected from the earlier numerical work of Chen (1975). To investigate the effects of ψ_1 values larger than those in the nominal spiral case while remaining within the constraints of the simulation model, the following assumptions were made: (a) at the shock-particle interaction point, the nominal ψ_1 is increased by a chosen factor to account for, for example, large-scale ($\gg$ energetic particle gyroradius) IMF fluctuations or non-spherical shock geometries; (b) particle motion from the shock to the observation point proceeds along the nominal spiral IMF. Numerical particle profiles generated under these assumptions are shown in Figure 5 (Decker, 1981).

The top panel in Figure 5 shows the numerically-generated intensity profiles for 0.46 and 1.0 MeV protons 'observed' in the solar equatorial plane at 1 AU when a 1000 km s^{-1}, $H = 4$ ($\eta = H$ in Figure 5) spherical shock passes through a 400 km s^{-1} solar wind (i.e., $|\mathbf{V}_{ss}| = 600$ km s^{-1}). A spatially uniform, isotropic pre-shock proton distribution of the form $\mathrm{d}J/\mathrm{d}T \propto T^{-\gamma}$, with $\gamma = 3$, was used. The shock passage is

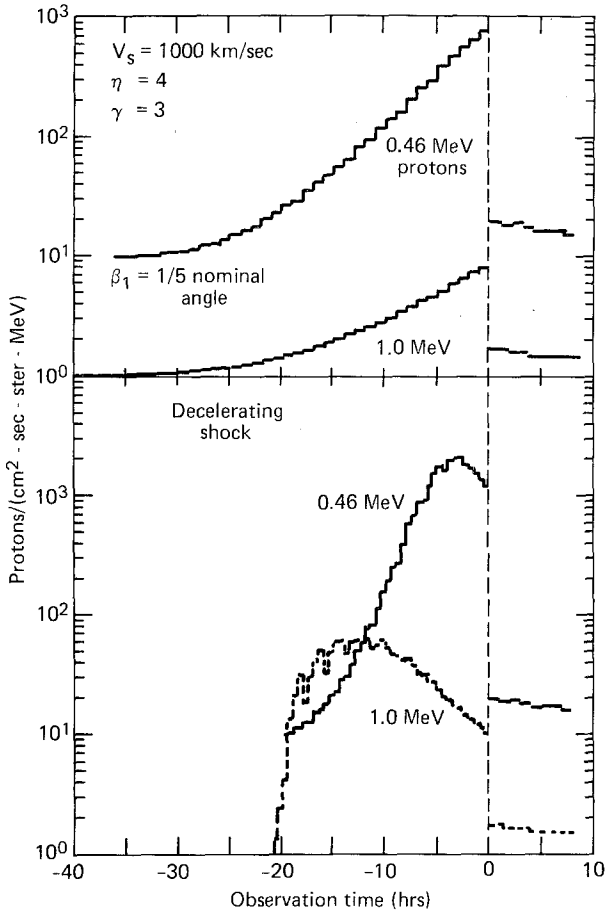

Fig. 5. *Top:* Flux-time profiles at 1 AU for a 1000 km s^{-1} strength 4 shock with $\beta_1 = 90° - \psi_1$ at the shock reduced to 1/5 the nominal spiral value. *Bottom:* Same as top panel except the shock decelerates from 2400 km s^{-1} at 0.1 AU to 1000 km s^{-1} at 1.0 AU and beyond.

indicated by the dashed vertical line. For the curves in both the upper and lower panels in Figure 5, $\beta_1 = 90° - \psi_1$ at the shock-particle interaction point was reduced to 1/5 the nominal spiral value. Thus, during the shock interaction, $\psi_1 \sim 81°$ at 1 AU and decreases towards the Sun. In the top panel of Figure 5 there is a steady build-up in particle intensity prior to the shock passage at time $t = 0$, and then a sudden decrease in intensity downstream of the shock. Notice that the peak to background intensity for 0.46 MeV protons is ~ 80, while that for 1.0 MeV protons is only ~ 8 at the shock passage. The gross features of the simulated intensity profiles and the variation of the peak to background intensities are consistent with many observations of ESP events.

The bottom panel in Figure 5 includes the effect of shock deceleration. The shock begins at 0.1 AU with a speed of 2400 km s^{-1} ($|\mathbf{V}_{ss}| = 2000$ km s^{-1}) and decelerates linearly with radial distance to a constant value of 1000 km s^{-1} ($|\mathbf{V}_{ss}| = 600$ km s^{-1}) at 1 AU. Peak to background enhancements of ~ 200 and ~ 60 occur ~ 3 hr and ~ 12 hr

prior to the shock passage for 0.46 and 1.0 MeV protons respectively. As the shock decelerates its ability to accelerate particles to $\sim$ MeV energies decreases. The position of the peak intensity is a function of both the time history of $|\mathbf{V}_{ss}|$ and the observer's distance from the shock. Because 0.46 MeV protons are more easily produced than 1.0 MeV protons for a given value of $|\mathbf{V}_{ss}|$, the 0.46 MeV peak occurs closer to the shock passage time and has a greater peak to background ratio.

The similarities between the upstream ESP intensity profiles in Figure 4 and the scatter-free simulation results in Figure 5 show that the separation of diffusive and guiding center effects require more information than the particle intensity time histories alone can provide.

The top (bottom) inset in the right-hand side of Figure 3 presents the downstream (upstream) pitch angle distribution observed during the hour immediately preceding (following) passage of the reverse shock. The distributions are constructed using one-minute averages of the interplanetary **B** and 0.11 s averages of the energetic proton data. The upstream distribution is anisotropic, field-aligned and directed away from the shock front (towards the Sun) along the nominal IMF. The downstream pitch angle distribution is anisotropic, peaked perpendicular to the field, and has a net field-aligned component which is directed away from the shock front (outward from the Sun) along the nominal IMF. Similar pitch angle distributions are usually observed in ESP events and SSE (see Table I). The effects of diffusive and guiding center propagation of the shock enhancement particles can best be studied by examining the relaxation of anisotropic particle pitch angle distributions as a function of distance from the shock, energy, particle species and IMF conditions. Isotropic diffusion shock acceleration models are of no use in the study of pitch angle relaxation. What is needed is a shock acceleration model that can handle arbitrarily large anisotropies.

6. Future Directions

A. Observations

(1) Use Voyager and ISEE data to construct data sets for shock events that extend continuously from solar wind to galactic cosmic ray energies. Include in the set data for electrons, protons, alphas and $Z > 2$ ions. In particular, a more comprehensive effort should be undertaken to search for shock-associated effects in the low energy electron data. [Potter (1981) has observed that electrons are routinely accelerated to $\gtrsim 2$ keV in ESP events at 1 AU.]

(2) Study the temporal and spatial evolution of two and three dimensional particle distribution functions using two or more spacecraft.

(3) Look for correlations between particle distribution functions and plasma wave and turbulence levels.

(4) Search for energetic particle modulation by slow-mode shocks.

B. NUMERICAL SIMULATIONS

(1) Study the effects of locally nonplanar shock fronts. Examine the effects of temporal and spatial variations in ψ_1 *during* the shock-particle encounters.

(2) Study the low velocity limit of the shock drift mechanism.

(3) Simulate the multiple shock encounter acceleration process.

(4) Study the effects that the global IMF and CIR geometries have upon large-scale features of CPE by combining the shock acceleration mechanism with particle transport models.

C. ANALYTICAL

(1) Develop models of thermal ion and electron acceleration in shocks.

(2) Develop models of energetic particle acceleration that combine the shock drift and compression mechanisms with a transport theory that can handle large anisotropies.

Acknowledgements

This work was supported at the University of Maryland by NASA Contract NRG 21–002–224 and APL 600109. Work at the Johns Hopkins University Applied Physics Laboratory and the University of Kansas was supported in part by NASA under Task I of Contract N00024–78–C–5384 between the Johns Hopkins University and the Department of the Navy and by subcontract to the Universities of Kansas, Maryland and Arizona and in part by NSF Grant ATM–79–25987. One of us (MEP) benefitted from conversations with E. Roelof and J. Earl.

References

Armstrong, T., Chen, G., Sarris, E., and Krimigis, S.: 1977, in M. Shea, D. Smart, S. Wu (eds.), *Study of Travelling Interplanetary Phenomena*, D. Reidel Publ. Co., Dordrecht, Holland, p. 367.

Axford, W., Leer, E., and Skadron, G.: 1977, *Proc. 15th Int'l Cosmic Ray Conf.* **11**, 132.

Barnes, C. and Simpson, J.: 1976, *Astrophys. J. Letters* **210**, L91.

Bell, A.: 1978, *Monthly Notices Roy. Astron. Soc.* **182**, 147.

Chen, G.: 1975, Ph.D thesis University of Kansas, Department of Physics and Astronomy.

Chen, G. and Armstrong, T.: 1975, *Proc. 14 Int'l Cosmic Ray Conf.* **5**, 5814.

Decker, R.: 1979, Ph.D thesis University of Kansas, Department of Physics and Astronomy.

Decker, R., Pesses, M., and Krimigis, S. M.: 1981, *J. Geophys. Res.* **86**, 8819.

Decker, R.: 1981, *J. Geophys. Res.* **86**, 4537.

Fermi, E.: 1949, *Phys. Rev.* **75**, 1169.

Fisk, L. and Lee, M.: 1980, *Astrophys. J.* **237**, 620.

Gloeckler, G., Hovestadt, D., and Fisk, L.: 1979, *Astrophys. J. Letters* **230**, L191.

Gosling, J., Asbridge, J., Bame, S., Feldman, W., Paschmann, G., and Sckopke, N.: 1980, *J. Geophys. Res.* **84**, 744.

Greenstadt, G. and Fredricks, R.: 1979, in L. J. Lanzerotti, C. F. Kennel, and E. N. Parker (eds.), *Solar System Plasma Processes III*, North-Holland, Amsterdam.

Ipavich, F., Pesses, M., and Weiss, H.: 1979, *EOS* **60**, 905.

McGuire, R., Van Hollebeke, M., McDonald, F., and von Rosenvinge, T.: 1980, *Bull. Am. Phys. Soc.* **25**, 597.

Northrop, T.: 1963, *The Adiabatic Motion of Charged Particles*, Interscience, New York.

Parker, E.: 1958, unpublished manuscript.
Parker, E.: 1963, *Interplanetary Dynamical Processes*, Interscience, New York.
Pesses, M.: 1982, *J. Geophys. Res.*, submitted.
Pesses, M. and Decker, R.: 1982, *J. Geophys. Res.*, submitted.
Pesses, M., Tsurutani, T., Van Allen, J., and Smith, E.: 1979, *J. Geophys. Res.* **84**, 7297.
Pesses, M., Van Allen, J., Tsurutani, T., and Smith, E.: 1982, *J. Geophys. Res.*, submitted.
Potter, D.: 1981, *J. Geophys. Res.* **86**, 11111.
Sarris, E. and Van Allen, J.: 1974, *J. Geophys. Res.* **79**, 4157.
Scott, J. and Pesses, M.: 1982, *J. Geophys. Res.*, submitted.
Smith, E. and Wolfe, J.: 1977, in M. Shea, D. Smart, and S. Wu (eds.), *Study of Travelling Interplanetary Phenomena*, D. Reidel Publ. Co., Dordrecht, Holland, p. 227.
Toptyghin, I. N.: 1980, *Space Sci. Rev.* **26**, 157.
Tsurutani, T.: 1980, private communication.
Zwickl, R. and Webber, W.: 1978, *J. Geophys. Res.* **83**, 1157.

Discussion

Anderson: What do you have to add to your model to account for the observed near-symmetry of the shock spike flux across the shock front?

Decker: The nearly symmetric shock spike events occur for a certain range of particle energies near quasi-perpendicular shocks. These events can be simulated for small angles between the upstream magnetic field vector and the shock normal (e.g., $\psi_1 \sim 88°$). Then the intensity enhancements due to upstream reflected particles and downstream transmitted particles can become nearly equal.

Lee: (Comment) I think Dr Anderson is referring to the ESP events which exhibit symmetric enhancements about the shock.

Dryer: Do I understand the terminology correctly? That is, a 'single' encounter could involve many (say, 18) helical revolutions through the shock before it leaves the shock. Then, later, scattering – due to turbulent irregularities upstream or downstream – could send the particle back to the shock for another 'single' encounter? And so on?

Decker: Yes, that's correct. By 'multiple shock encounters' I mean that the particle encounters the shock two or more times, with each encounter involving many orbital crossings of the shock front.

Ivanov: Could you comment on particle acceleration by plasma turbulence behind the shock front?

Decker: Magnetic field turbulence behind the shock front could scatter particles and enable them to encounter the shock several times. The simulated particle enhancement profiles are for the simple case of laminar magnetic fields upstream of the shock. Therefore, scattering effects have not been taken into accδunt in the numerical calculations.

Lee: Can these particle enhancements be explained by a single encounter with the shock?

Decker: Not always. For the shock spike events and some ESP events a single encounter seems adequate to produce the observed enhancements. For larger ESP events and the CPE structures in particular, multiple encounters are necessary to produce such large intensity enhancements.